Thermally Driven Ag−Au Compositional Changes at the Ligament Surface in Nanoporous Gold: Implications for Electrocatalytic Applications

Mareike Haensch, Matthias Graf, Weijia Wang, Alexei Nefedov, Christof Wöll, Jörg Weissmüller, and Gunther Wittstock*

ABSTRACT: Nanoporous gold (NPG) is a versatile, nanoporous bulk material with applications in catalysis, sensors, energy materials, and actuation. NPG obtained from dealloying Ag rich Au−Ag alloys has interesting applications in electrocatalysis, for which methanol oxidation is an interesting test case. Such materials always contain a content of residual silver which may play a role in activating and binding of reaction intermediates. The residual Ag that is contained in NPG due to the dealloying of a Ag−Au alloy was recently found to be present in silver rich islands, in contrast to being homogeneously distributed. Because of the importance of residual Ag on the surface science and catalytic properties of NPG, we investigated its distribution and chemical nature with the use of X ray photoelectron spectroscopy. During the in situ annealing, changes of the near surface content of residual Ag were observed, and they were linked to coarsening of the gold ligaments. In addition, a depth dependent analysis of synchrotron based XPS results confirmed the surface segregation in the near surface layers of each ligament. The available data neither confirm nor exclude a further systematic enrichment or depletion of silver in the topmost atomic layer for NPG during electrochemical treatments in KOH solution or during thermal coarsening.

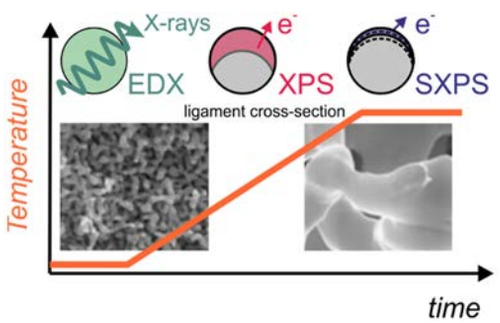

KEYWORDS: *nanoporous gold, dealloying, residual silver, surface concentration, X ray prohotoelectron spectroscopy, synchrotron radiation photoelectron spectroscopy, surface segregation, annealing*

INTRODUCTION

Nanoporous gold (NPG) is a material that attracts the attention of researchers in fields as diverse as actuation,[1,2] energy conversion and storage,[3] sensing,[4,5] and (electro) catalysis.[6,7] It consists of a bicontinuous network of gold ligaments and pores with sizes in a widely tunable range. It shows metal like thermal and electrical conductivity besides high mechanical strength[8] and surprising catalytic activity.[8] The large surface to volume ratio is obtained by high curvature ligaments and provides a huge number of active sites for (electro)catalytic reactions. To understand the high catalytic activity of this material, surface composition and structural properties are intensively investigated.[9−12] NPG is commonly fabricated via "dealloying", i.e., leaching the less noble component from a Au alloy (e.g., Au−Ag). Depending on the applied dealloying method, NPG contains varying mole fractions of residual Ag (x_{Ag} = 1−12%).[13] The mole fraction of residual Ag in NPG prepared by potentiostatic dealloying is linked to the ligament size: The smaller the ligament size, the higher is the residual Ag.[9,14] Concurrent surface diffusion of Au atoms under corrosive conditions uncovers previously protected Ag atoms which are then dissolved.[14] Thus, the interplay between Au surface diffusion rate and Ag dissolution rate is an important factor controlling the residual Ag content. Here, we consider the distribution of residual Ag within ligaments, its changes with different thermal and electro chemical treatments, and the consequences for a canonical case of electrocatalytic reactions, namely, the oxidation of methanol.

By means of scanning transmission electron microscopy (STEM) and reconstructed energy dispersive X ray spectros copy (EDX), it has been recently discovered that part of the residual Ag occurs as regions with a composition similar to that of the parent alloy within the NPG ligaments.[10,14] These remnants from the parent alloy are preserved during dissolution when Au atoms passivate the surface and prevent further Ag dissolution.[14] Therefore, NPG cannot be consid ered a homogeneous alloy, but Ag is unevenly distributed, resulting in potential effects on (electro)catalysis. A density

functional theory (DFT) approach proposed that NPG with low concentrations of residual Ag can activate oxygen by adsorption from the gas phase. According to the authors, this is considered the basis of the oxophilicity of NPG and its catalytic activity toward many oxidation reactions.[15] Moreover, DFT calculations suggest that Ag at the surface can also stabilize chains of gold oxides, which in turn may also favor Ag segregation to the surface.[16] Small concentrations of residual Ag are of particular interest for partial oxidation reactions.[10,17]

Different techniques have already been employed to study the composition of NPG (Scheme 1). Among them, EDX with an information depth of ~1 μm (i.e., much larger than the diameter of a ligament) is commonly used to determine total concentrations of residual Ag.[18−20] X ray photoelectron spectroscopy (XPS) has been used for studying the near surface composition of NPG on several occasions.[21,22] Because (electro)catalytic reactions take place at the NPG−solution interface, surface sensitive concentration measurements (as obtained by XPS) are of high importance for correlating reactivity and composition. In our previous publication, we demonstrated changes in both the near surface composition and the chemical state of residual Ag during electrochemical methanol oxidation at NPG.[6] Studies on planar Ag−Au alloy surfaces revealed that Ag is enriched in the first few nanometers of the surface,[23,24] probably because of the lower surface free energy of Ag (1.24 J m^{-2}) in comparison to Au (1.50 J m^{-2}).[25] It has also been pointed out that oxygen may promote Ag segregation.[26]

In this study, we investigate the near surface composition of NPG and the chemical states of residual Ag during thermal annealing. Besides laboratory XPS using monochromatized Al Kα radiation, we performed synchrotron based XP spectros copy (SXPS) studies to further increase the surface sensitivity of XPS and to obtain information about the depth distribution of residual Ag by variation of the kinetic energy of the emitted electrons in the range 150−320 eV.

EXPERIMENTAL SECTION

Preparation of Nanoporous Gold. NPG cylinders (height h = 2 mm, radius R = 0.5 mm) were prepared from $Ag_{72}Au_{28}$ alloy cylinder samples prepared by arc melting and subsequent tempering of the obtained ingot at 925 °C for 100 h under Ar to homogenize the Ag−Au alloy by bulk diffusion.[27] After cooling, a wire was drawn stepwisely being repeatedly interrupted by thermal curing at 650 °C for 5 min. Finally, the wire was cut by sawing. A multistep potentiostatic dealloying according to Graf et al.[9] was applied in 1 M $HClO_4$ with a Ag wire as auxiliary electrode and an Ag|AgCl|3 M KCl reference electrode. NPG was obtained after dealloying at 1.05 V vs Ag|AgCl|3 M KCl (for 24 h) followed by 1.10 V (8 h), 1.15 V (8 h), and finally 1.20 V (10 h). After this program the potential was switched back to open circuit; samples were taken out of the cell and washed in deionized (DI) water. The samples were stored in DI water for 1 day. Samples NPG 300 and NPG 100 were then dried, packaged, and shipped under Ar. After arrival at the XPS instrument, the samples were transferred to the ultrahigh vacuum (UHV) chamber with a base pressure of (1−2) × 10^{-9} mbar. The samples were heated in the UHV chamber of the XPS instrument to 300 and 100 °C and further denoted as "NPG 300" and "NPG 100", respectively. The exact temperature was measured by a thermoele ment attached to the sample and is given Figures 1A and 4A.

Samples for the SXPS experiments (Table 1) were treated differently after the washing step. The sample code is a shorthand for those treatments. The electrochemical pretreatment was performed in a three electrode cell with NPG as working electrode, a Ag wire as auxiliary electrode, and a Hg|HgO|1 M KOH reference electrode. The electrochemical experiment was an amperometric oxidation (character "A" in the code) or the application of 100 potential cycles (character "C" in the code) in an aqueous solution of 1 M methanol and 1 M KOH (character "M" in the code) or in 1 M KOH solution without methanol (digit "0" in the code). Further details are summarized in Table 1. Sample NPG T was thermally annealed at 300 °C for 1 h without exposure to alkaline solution.

XPS Experiments. *Heating Experiment.* Nanoporous gold cylinders were cleaved with a scalpel to expose the cross section for analysis and directly transferred to the XPS chamber of an ESCALAB 250Xi instrument (Thermo Fisher Scientific, East Grinstead, UK). A special sample holder with a heater and a thermoelement was used for following the spectra during annealing. The temperature was ramped from RT to 300 °C and held constant to acquire Ag 3d and Au 4f spectra with a pass energy of 10 eV at the same temperature. The base pressure of the XPS chamber was (1−2) × 10^{-9} mbar. During the

Scheme 1. Schematic Representation of the Information Depth of EDX, XPS, and SXPS as Applied in This Study to NPG[a]

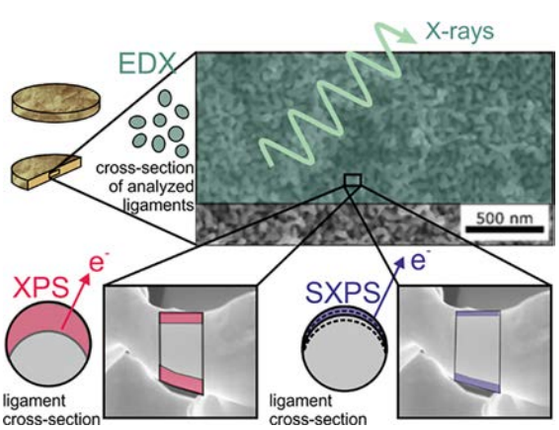

[a]Below the acronym, the analyzed region is colored within a schematic of a cross section of a ligament or several ligaments in the case of EDX. In the insets, the analyzed regions are colored as well.

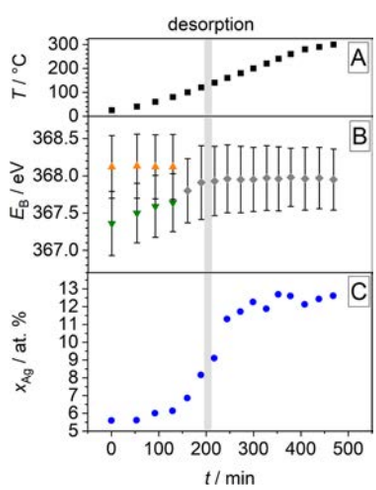

Figure 1. (A) Temperature ramp and extracted data from the Ag $3d_{5/2}$ spectra. (B) E_B for the peak components Ag^0 (▲), Ag_{ox} (▼), and single Ag component (◆); the vertical bars indicate the fwhm of each component. (C) Residual Ag mole fraction x_{Ag} as determined by quantification of the Ag $3d_{5/2}$ and Au $4f_{7/2}$ peaks. The gray line indicates the time where a major fraction of surface contaminants are desorbed from the surface according to the residual gas analysis (RGA) results (see section Supporting Information 1).

Table 1. Code and Sample Pretreatment for SXPS Investigation[a]

no. in Figure 7	code	treatment after dealloying	ligament size (nm)
1	NPG-C0	100 potential cycles in 1 M KOH between 0.5 and +1.3 V; ν = 0.01 V s^{-1}	35 ± 6
2	NPG-CM	100 potential cycles in 1 M methanol + 1 M KOH between 0.5 and +1.3 V; ν = 0.01 V s^{-1}	37 ± 6
3	NPG-A0	5 min in 1 M KOH at +0.55 V	34 ± 8
4	NPG-AM	5 min in 1 M methanol + 1 M KOH at +0.55 V	39 ± 6
5	NPG-T	thermally annealed at 300 °C for 1 h	480 ± 120

[a]All potentials refer to a Hg|HgO|1 M KOH reference electrode.

heating experiment, the vacuum system limits pressure rises to 2 × 10^{-6} mbar when compounds desorb. The pressure during measure ments using the charge compensation was 2 × 10^{-7} mbar.

Synchrotron-Based XPS. SXPS was performed at room temper ature at the HE SGM[29] beamline of the synchrotron facility BESSY II, which is a part of Helmholtz Zentrum Berlin (Berlin, Germany). The Scienta R3000 electron analyzer (VG Scienta, Uppsala, Sweden) was used with a pass energy of 20 eV during the experiments.

Data Treatment. Both XP and SXP spectra were fitted with the software Avantage v5.932 (Thermo Fisher) by using a smart background (i.e., a modified Shirley) and fitting the peaks by multiplication of Gaussian and Lorentzian contribution. Spectra acquired at the ESCALAB instrument ($h\nu$ = 1486.6 eV) were quantified by using the sensitivity factors from the internal library of the instrument. For spectra acquired at the HE SGM beamline, peak areas were corrected by the photon flux, the photoionization cross sections for the specific incident photon energy according to Band et al.,[28] and the mean free path length.[29] Details are given in section SI 5 for SXPS and section SI 6 for XPS.

SEM and EDX Analysis. SEM micrographs of samples before and after annealing were obtained at a Helios Nanolab 600i system (FEI Company, Hillsboro, OR). The EDX analysis of these samples was performed at a Leo Gemini 1530 microscope (Carl Zeiss Microscopy GmbH, Jena, Germany). Samples prepared for SXPS experiments were investigated with SEM and EDX after the experiment using the Leo Gemini 1530 microscope. At selected samples, EDX measure ments were performed at five different locations. The results are stated as an arithmetic mean and a standard deviation which may give an approximation for the reproducibility of those measurements with the studied sample and measurement parameters.

Ligament sizes were determined from SEM images at 250000 fold magnification as described in ref 9. In brief, the widths of 20 ligaments intersected by a diagonal of the image frame were measured by using the software Gwyddion v.2.45[30] and averaged. Values are reported as arithmetic mean ± standard deviation.

RESULTS AND DISCUSSION

Changes of Surface Composition of NPG during Heating in a Vacuum. Ag rich regions within NPG ligaments[10,14] are expected to equilibrate during thermal annealing, which may be accompanied by a redistribution of Ag between the bulk of the ligaments and their surfaces. Here we follow this process by recording XP spectra simultaneously to the thermal treatment in a vacuum. A NPG sample in the shape of a cylinder (1 mm diameter, 2 mm height, denoted as NPG 300) was fabricated as described earlier[9] and stored under inert gas. The cross section of the brittle samples was exposed for XPS investigation by cleavage using a scalpel, after which the sample was directly transferred into the XPS analysis chamber of the laboratory instrument. Because of the high ductility of Au, cleavage of NPG occurs by thinning ligaments across the fracture plane until connection is lost. Although new surface is generated in this process, cross sections of individual ligaments are rarely exposed as evident from the SEM images in this work as well as in other studies.[31] The effect of the newly exposed surface seems small as judged by the SEM images and is further reduced if the sample is subjected to thermal treatment in a vacuum. Ag $3d_{5/2}$ XP spectra were recorded with a steplike increase of temperature starting from room temperature (RT) up to 300 °C (Figure 1A). A selection of the obtained spectra is presented in Figure 2. For the as dealloyed (i.e., not annealed) NPG sample, two Ag $3d_{5/2}$ components are discerned (Figure 2A) and assigned to Ag^0 (368.1 eV) and AgO (367.4 eV).[32] Generally, the Ag 3d peaks in NPG are shifted to slightly lower binding energies E_B than in pure Ag (368.20 eV) as observed before for binary Ag−Au alloys of different composition.[33] The lower the fraction of Ag in the alloy, the lower is E_B. In our previous work, we could

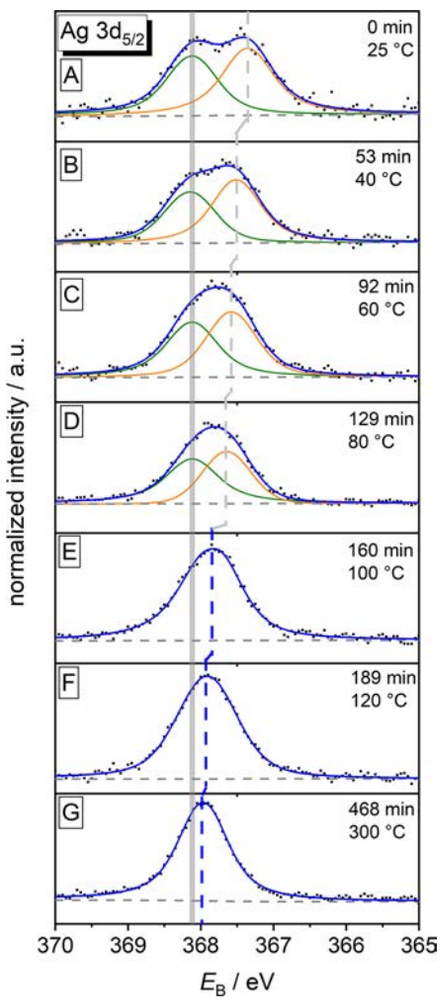

Figure 2. Ag $3d_{5/2}$ XP spectra recorded at different temperatures during the thermal annealing of a NPG cylinder (NPG 300): (A) as dealloyed at RT, (B) T = 40 °C (t = 53 min), (C) T = 60 °C (t = 92 min), (D) T = 80 °C (t = 129 min), (E) T = 100 °C (t = 160 min), (F) T = 120 °C (t = 189 min), and (G) T = 300 °C (t = 468 min). The experimental data points are plotted as dots, the envelope as a blue line, single components as orange and green lines, and the background as a dashed line. The solid gray vertical line indicates Ag^0 at E_B = 368.1 eV, and the dashed vertical line indicates the shift of the Ag oxide component (A−D) and the Ag peak (E, F).

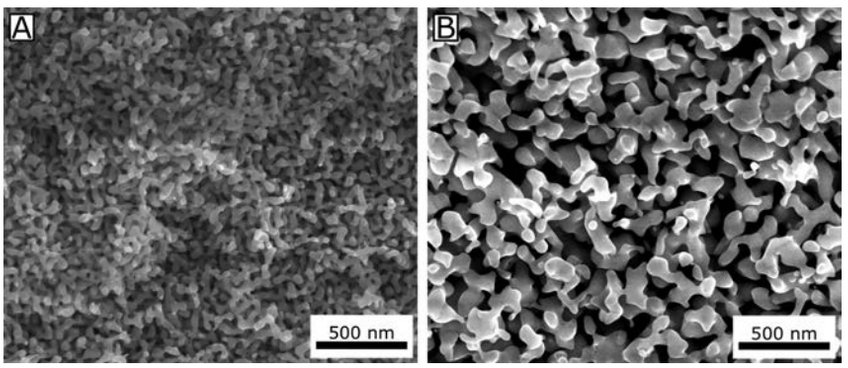

Figure 3. SEM images of cross sections of NPG 300 before (A) and after (B) thermal annealing up to 300 °C in a vacuum.

reproduce these results on electrodeposited Ag−Au alloy films and calibrate shifts of E_B to the silver content of the alloy.[6] With increasing temperature, the AgO component shifts to higher E_B as indicated by the dashed line in Figure 2A−D. At 80 °C, E_B was found at 367.6 eV, which can be attributed to the decomposition of AgO to Ag_2O and O_2 (Figure 2D). Ag_2O is known to decompose already at moderate temperatures of 83−200 °C.[32,34]

At temperatures above 80 °C (Figure 2E−G) no distinction between Ag^0 and Ag oxides can be made, although the broader peak width and its lower E_B suggest a superposition of two components corresponding to Ag and Ag oxide. The results of the peak analysis are shown in Figure 1B. Above 120 °C the peak position (E_B = 367.9 eV) remains relatively constant (dashed blue line in Figure 2E−G) while the full width at half maximum (fwhm) decreases from approximately 0.99 to 0.84 eV, a value equal to that of the Ag^0 component in the as dealloyed state. This indicates a rather defined chemical environment with mainly Ag^0 present at the final temperature. As mentioned above, it was shown that the shift of E_B(Ag) in Ag−Au alloys depends on the mixing ratio of both elements.[6] Therefore, E_B is indicative for the local Ag mole fraction around the emitter atom. The observed shift in E_B(Ag) is therefore a consequence of rearrangement of atoms within the NPG crystal lattice during thermal treatment. In this process Ag atoms move from regions with high local concentration to regions with lower local concentration. This observation is in agreement with the finding that NPG in its state after dealloying contains Ag rich regions within the ligaments. These Ag rich regions equilibrate with the Ag poor, Au rich matrix during heating by surface diffusion.[14]

The temperature at which this rearrangement occurs coincides with that of the decomposition of surface oxides and the desorption of organic contaminations and water. Desorption was observed in situ by mass selective residual gas analysis in the XPS analysis chamber (section SI 1). Initially, water is released from the surface followed by CO, CO_2, and O_2 which indicate decomposition of surface oxides and the simultaneous oxidation of organic contaminations. The oxides decompose at the same temperature at which both ubiquitous organic contaminations are oxidized and Ag rich regions within the ligaments equilibrate with the surrounding Ag poor matrix. This coincidence suggests oxidation of the organic contaminations by Ag oxides and an increased surface mobility of atoms in the metallic state compared to the oxidic state. This increased mobility is a prerequisite for the observed atomic rearrangements during equilibration of the Ag rich islands present in the as dealloyed NPG samples. Although the formation of Ag_2CO_3 from initially formed Ag_2O and CO_2 from an ambient environment is conceivable, no signature of Ag_2CO_3 were found in the Ag 3d and C 1s high resolution scans.

Before and after the thermal annealing of the NPG 300 sample in the XPS analysis chamber, SEM images were recorded (Figure 3). As it was shown in the literature before, the porous structure is preserved during the annealing.[35] The mean diameter of the ligaments increased from L_B = 32 ± 8 nm in the as dealloyed state to L_B = 74 ± 26 nm after thermal annealing. To achieve a more than 2 fold increase, a large number of atoms have to diffuse to rebuild the ligaments. The movement of atoms over relatively large distances enables the change in a chemical composition in the near surface region. The EDX bulk analysis yields an Ag mole fraction x_{Ag} of 4.2 ± 0.8% after the annealing as compared to 5.4 ± 0.6% before annealing. Within the uncertainty of EDX, the x_{Ag} remains constant. The uncertainty range of EDX data was determined from multiple measurements of identical samples at slightly varied beam positions. The values are also in agreement with the XPS analysis of NPG in the as dealloyed state (5.6 ± 0.5%). The experimental uncertainty of the XPS data can be estimated from the repeated analysis of the same sample during the heating experiments when no further changes occurred (Figure 1C, t = [300 min, 450 min], and Figure 4, t = [150 min, 640 min]). This value is about ±0.5% in x_{Ag} in the relevant concentration range (5% relative error). This value is better than uncertainties typically quoted for quantitative XPS

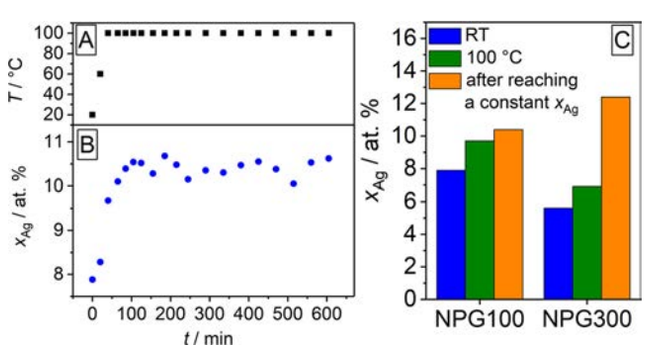

Figure 4. Changes of local surface composition: NPG 100 with (A) temperature program and (B) x_{Ag} as determined by quantification of Ag $3d_{5/2}$ and Au $4f_{7/2}$ peaks. (C) Comparison of x_{Ag} from XPS for the samples NPG 100 and NPG 300 at room temperature (blue bars), at 100 °C (green bars), and 60 min after reaching the constant concentration (orange bars).

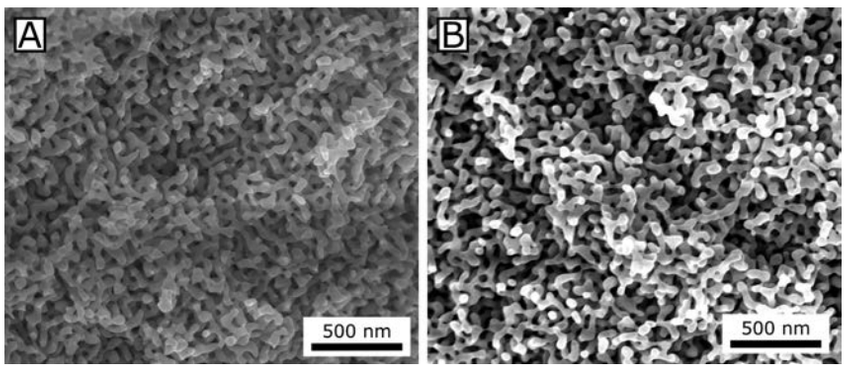

Figure 5. SEM images of the cross section of NPG 100 (A) before and (B) after thermal annealing at 100 °C in a vacuum.

analysis because the sample with two noble metals is particularly favorable for XPS analysis (large excitation cross section, small line width, and clearly separated signals). Small lateral variations of local x_{Ag} in the nanometer range are averaged within the excitation area of XPS or SXPS.

To investigate the influence of annealing temperature and annealing duration on NPG properties, a NPG sample (denoted as NPG 100) was quickly heated to 100 °C and then held at this temperature for 640 min (Figure 4) to reach the same total annealing time as for sample NPG 300. The temperature dependent change of NPG properties is very similar as in the experiment described in Figure 1: A rapid change in near surface Ag concentration is detected at around 100 °C (Figure 4B). The development of near surface Ag mole fraction is compared in Figure 4C for samples NPG 100 and NPG 300 at RT and 100 °C and after reaching a constant concentration. The relative change in x_{Ag} at 100 °C amounts to 23% for both samples. However, the detailed analysis of the spectra reveals that higher temperatures are needed for further changes in x_{Ag} which cannot be achieved by prolonged annealing at 100 °C despite the observation of small compositional changes detected in this situation.

The SEM images of the NPG 100 sample after annealing reveal no coarsening (ligament sizes in dealloyed state are L_B = 39 ± 10 nm and after annealing L_B = 37 ± 9 nm, Figure 5), and only rather small changes of the x_{Ag} occur on the surface at the beginning of the annealing process, which remain constant with further treatment over 640 min at that temperature (Figure 4B). There are no morphological changes after annealing at 100 °C in a vacuum for 60 min (Figure S2), a time at which most of the compositional changes at the surface had been completed in Figure 4B. To achieve an even stronger change of x_{Ag} such as in sample NPG 300 (Figure 4C), higher temperatures are required that also accelerate coarsening significantly as shown in Figure 3B. The segregation of Ag in Ag−Au alloys has been found to occur within a few nanometers from the surface.[23,24] The regular solution model[36] predicts that the surface enrichment factor, i.e., the ratio between x_{Ag} at the surface (here measured by XPS) and the x_{Ag}* in the bulk (here obtained from EDX data), depends on the surface energies and the total concentration of Ag. For alloys with a strong tendency for segregation, and for not too dilute solutions in the bulk, the simple regular solution model predicts that the surface enrichment factor increases with decreasing solute content in the bulk. Our observations on NPG with low Ag concentrations and strong surface segregation during annealing are in good agreement with results presented in ref 23, where a ratio of $x_{Ag,surface}/x_{Ag,bulk}$ = 2.5 was found for the Ag total mole fraction x_{Ag} = 10%.

Residual Ag is assumed to be at least in part responsible for the high catalytic activity of nanoporous gold because Ag can better activate oxygen than Au. However, previous studies have shown that especially samples with low residual Ag content showed high catalytic performance.[6,37] Because there is also a correlation between x_{Ag} and the ligament size,[9,14] it is unclear whether the effect of x_{Ag} on the (electro)catalytic activity for partial oxidation reactions of alcohols (such as shown in Figure S3) is due to the adsorption or interaction of reaction intermediates with surface Ag atoms or whether this effect is an indirect consequence of the larger ligaments which coincide systematically with small x_{Ag}. Because larger ligaments only exist when separated by larger pores, such samples could lead to lower diffusional hindrance in liquid reaction mixtures and thus higher performance.

Silver Mole Fraction in the Topmost Atomic Layers. The topmost atomic layer is involved in binding reaction intermediates and thus is likely to be relevant for electro catalysis. When NPG is used as electrode for electrocatalysis, further deviation from the Ag surface enrichment (shown in Figures 1 and 4) may occur in the topmost atomic layer due to reactions at the solid−liquid interface such as dissolution of the less noble metal. Surface oxidation, or binding of OH^-, or binding of reaction intermediates (e.g., from methanol oxidation) may promote further surface enrichment. Such changes in surface properties of NPG are evident from the cyclic voltammograms of samples in 1 M KOH and in 1 M methanol +1 M KOH (Figure S3). In 1 M KOH the signals are visible for surface oxidation and surface oxide reduction. The surface oxide reduction peak decreases in Figure S3 with cycle number indicating a loss of electrochemical surface area, i.e., coarsening. Although clearly visible, this effect is *much* smaller than during electrochemical cycling in acidic electrolyte solutions. When cycling in 1 M methanol + 1 M KOH, the electrocatalytic oxidation wave at +0.6 V (vs Hg|HgO) in the positively going scan is visible. It also decreases with cycle number while the surface oxide reduction peak remains essentially constant (Figure S3). For prolonged cycling of samples in 1 M methanol + 1 M KOH the peak current for methanol oxidation decreases (Figure S4). For comparison of as dealloyed samples and samples after a heat treatment at 100 °C in a vacuum for 60 min, the peak currents were normalized to the mass of the specific NPG sample. For both samples a very similar trend was observed.

To estimate the influence of Ag content at the surface of NPG on electrocatalysis, it is desirable to know the surface

concentration. Even XPS data with an information depth of 5.2 nm for Au 4f and 4.6 nm for Ag 3d photoelectrons may significantly deviate from x_{Ag} in the topmost layers of NPG. SXPS experiments were performed to gain more information about the depth dependent concentration of residual Ag by variation of the photon energy between 234 and 400 eV (for Au 4f) and between 518 and 684 eV (for Ag 3d). As dealloyed samples were treated as detailed in Table 1 before being prepared for SXPS measurements. In addition to the program used for the cyclic voltammograms from which Figure S4 was compiled, oxidation at constant potential and heat treated samples were tested. The SEM images of all samples are shown in Figure S5. Exemplary spectra are shown in Figure 6. The change of excitation energy results in a change of the kinetic energy E_{kin} of excited electrons, which causes changes of the inelastic mean free path length λ of the photoelectrons and thus of the information depth of the analysis (section SI 5).

The bulk Ag mole fraction (Figure 7, horizontal lines) and the ligament sizes (Table 1) were determined from EDX and SEM experiments, respectively. The ligament size of the samples NPG A0, NPG AM, NPG C0, and NPG CM were very similar to each other. This is in agreement with our earlier

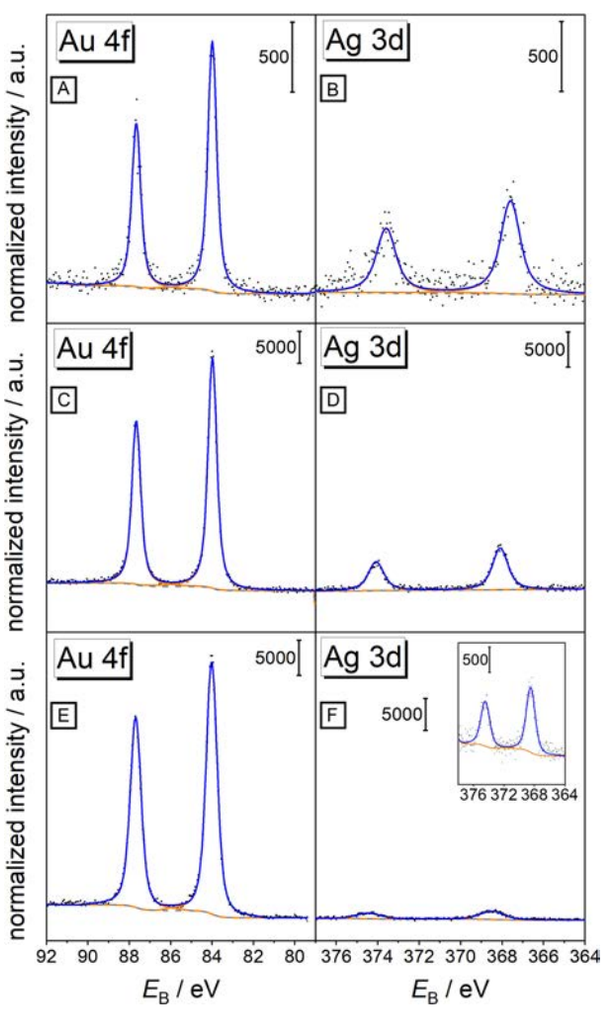

Figure 6. Exemplary SXP spectra of Au 4f and Ag 3d in NPG A0 recorded at (A, B) E_{kin} = 150 eV ($h\nu$ = 234 eV), (C, D) 216 eV ($h\nu$ = 300 eV), and (E, F) 316 eV ($h\nu$ = 400 eV). The inset in (F) shows the enlarged Ag 3d spectrum.

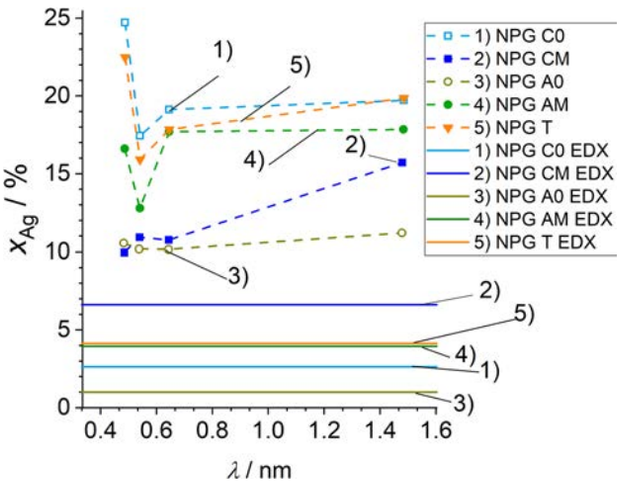

Figure 7. Quantification of x_{Ag} as a function of inelastic mean free path length in SXPS and XPS investigation. The results of EDX are considered as bulk values and are given as horizontal solid lines. Dashed lines between SXPS and XPS data are a guide to the eye. The numbers at the curve refer to the legend and Table 1 detailing the treatment of the samples after dealloying.

work,[6] where CV cycles of methanol electrooxidation did cause less coarsening than in acid solutions.[38] The thermal annealing of sample NPG T resulted in significant coarsening of the ligaments to 480 ± 120 nm (Table 1). As expected, the bulk Ag mole fraction (as determined from EDX) $x_{Ag,EDX}$ = 4.1% was not influenced by thermal annealing. All five samples in Table 1 showed bulk Ag mole fractions within the variability limits of the used dealloying procedure (Figure 7).

The photoelectrons in Figure 6 had kinetic electron energies E_{kin} of 150, 216, and 316 eV. Note that the lowest photon energy available at this beamline is 153 eV with very low intensity that would result in $E_{kin} \approx 70$ eV for Au 4f. However, this excitation is unfavorable not only because of the low intensity but also because of an overlap with a Au Auger line. Therefore, E_{kin} = 150 eV was selected as the energy providing the smallest information depth in this study. Even at this photon energy, the signal to noise ratio for the Ag 3d and Au 4f spectra measured is relatively low (Figure 6A,B). Because of low signal to noise ratio in the spectra, a pass energy of 20 eV had to be chosen which resulted in broader peaks (compared to Figure 2) which prevented a sensible peak fitting of closely spaced Ag 3d components. As the information depth is increasing in Figure 6, the relative intensity of the Ag 3d line is strongly decreasing. This effect is mainly caused by the strongly different photon fluxes used to record the Au 4f spectra in the range of $h\nu$ between 234 and 400 eV (section SI 5). The quantification must take into account the different photon flux $J(h\nu)$ at different X ray energies (Figure S6), the change of the inelastic mean free path length λ with E_{kin}, the material density,[29] and the dependence of the atomic sensitivity factor σ_{ij} on the photon energy (Table S3).[28] The details of the quantification are summarized in section SI 5. The resulting differences of λ for NPG samples with slightly different compositions are only small for fixed photoelectron energy E_{kin}. They can be observed as slightly different positions of the data points in Figure 7. It should be noted that λ is much smaller than the ligament sizes listed in Table 1; thus, SXPS and XPS provide information about the near surface

composition of ligaments exposed by fractioning macroscopic monoliths (Scheme 1).

The elemental concentration is given for each sample as a function of λ in Figure 7. The three data points at 0.48 nm < λ < 0.65 nm are obtained from SXPS measurements for each sample; the data point at $\lambda \approx 1.5$ nm was recorded at the same samples with a laboratory XPS instrument using Al Kα radiation. The EDX values are assumed to represent the average bulk concentrations x_{Ag}*, which are given as horizontal lines in Figure 7. The SXPS values are approximately equal to the XPS values within the uncertainty of the SXPS method. All x_{Ag} from SXPS and XPS are larger than the $x_{Ag,EDX}$ from EDX as already shown in Figure 1. We consider this as a result of surface segregation of Ag.

Although it seems that there are different x_{Ag} values from SXPS and XPS data between individual samples, no clear trend with respect to the post dealloying treatment in Table 1 can be identified that can be separated from variations in the dealloying process, uncertainties of the photoelectron spectros copies and uncertainties that enter into the concentration calculation via used constants (sections SI 5 and SI 6). Likely, the variation in x_{Ag} levels between samples stems from the original dealloying process itself because also the EDX results show a variation between 1% and 7% despite a uniform dealloying protocol. Interestingly, the same trend is found for a sample that was thermally annealed in air after dealloying and showed the expected coarsening (Figure S5E). In this sample, the overall composition cannot change as opposed to leaching for electrochemically treated samples. Thus, changes of surface composition in sample NPG T must result from surface segregation.

The surface enrichment factor $x_{Ag,XPS}/x_{Ag,EDX}$ seems to increase with decreasing bulk Ag content (Figure 8) independently of the particular electrochemcial post dealloying treatment. Similar plots for the x_{Ag} values derived from SXPS data show the same trend with more scatter. The correlation between the surface enrichment factor and the bulk Ag content seems to be quite strict in Figure 8. Interestingly, the value for the sample NPG 300 (annealing in a vacuum) fits exactly to the data in Figure 8 for electrochemcially treated samples or the sample NPG T annealed in air. Oxygen and oxygen containing species (H_2O, OH^-) would be expected to

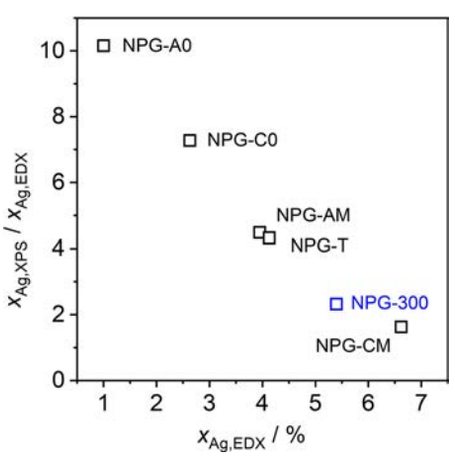

Figure 8. Surface enrichment factor calculated from $x_{Ag,XPS}$ and $x_{Ag,EDX}$ for the samples in Figure 7 (black) and Figure 2 (blue) as a function of their $x_{Ag,EDX}$ (representing the bulk Ag content).

additionally promote Ag surface segregation for the samples in Figure 8. However, our data cannot confirm this.

The surface enrichment of Ag bears important implications for (electro)catalysis as reaction intermediates bind to the topmost atomic layer, and the residual Ag is believed to play an important role in the activation of oxygen containing intermediates. Surface spectroscopic techniques, which are often used to correlate the residual Ag content at the surface with reactivity data (e.g., from voltammetry), provide concentrations that are integrated over the sample depths (eqs S1 and S6). The reconstruction of concentration profiles by variation of the inelastic mean free path length λ allows the reconstruction of profiles if the decay length of the concentration profile $y_{Ag}(z)$ is larger than the largest λ applied. In those cases, the experimental values $x_{Ag}(\lambda)$ are expected to agree with the local concentrations $y_{Ag}(z = \lambda)$ (Figure S7E,F).

Electrochemical treatments are prone to further alter the surface composition by dissolution of the less noble metal, the enrichment of the less noble metal in surface and subsurface oxide layers, or the preferential adsorption of reaction intermediates to one of the constituting metals. It is therefore conceivable that the concentration profile $y_{Ag}(z)$ of NPG electrodes is formed by a bulk content of residual Ag, a surface enrichment caused by dealloying and further thermal or electrochemical treatment as detected by XPS (Figure 8), and a further variation that affects only the topmost atomic layers. To elucidate how SXPS and XPS would sense such profiles, we calculated biexponential concentration profiles using eq S5 and then calculated the resulting SXPS and EDX intensities using eqs S6 and S7. An example of such a comparison is shown in Figure 9, for which the bulk Ag mole fraction y_{Ag}* was 4% for all profiles and is given as horizontal black line (i.e., this would be the EDX data). The profile in Figure 9C shows a monoexponential decay of $y_{Ag}(z)$ from 16% at the surface to the bulk value y_{Ag}* = 4% with a decay constant β_1 = 2 nm. In this situation, SXPS and XPS derived mole fraction $x_{Ag}(\lambda)$ at depth λ would follow exactly the assumed concentration profile $y_{Ag}(z = \lambda)$ because the decay length β_1 of $y_{Ag}(z)$ is larger than λ for SXPS and XPS. This is not the case if an additional concentration gradient is overlaid with a much shorter decay length (β_2 = 0.574 nm) corresponding to two atomic layers in NPG. Only if the associated pre exponential factor $y^0_{Ag,2}$ assumes large values may the concentration profile at the very surface be reconstructed semiquantitatively (Figure 9A,E,F). For smaller variations such as $y^0_{Ag,2}$ = [−6%; +6%] in Figure 9B,D, no clear distinction vs the monoexponential decay in Figure 9C is possible from the SXPS and XPS. The profiles in Figure 9B−D show a variation of the surface concentration $y_{Ag}(z = 0)$ between 10% and 22%, yet the expected SXPS and XPS data show only changes that are probably within the uncertainty range of an individual measurement. Note that SXPS and XPS intensities plotted in Figure 9 were calculated for idealized conditions without any experimental uncertainty. In real experiments, uncertainty ranges for individual data points would add to the complications. The difficulties increase as the decay length β_2 of the concentration change decreases at the very surface. Figure S9 shows analogous profiles when the decay length of β_2 = 0.287 nm corresponds to only one atomic layer. In this case the uncertainty in estimating the actual Ag mole fraction in the topmost atomic layer increases even further.

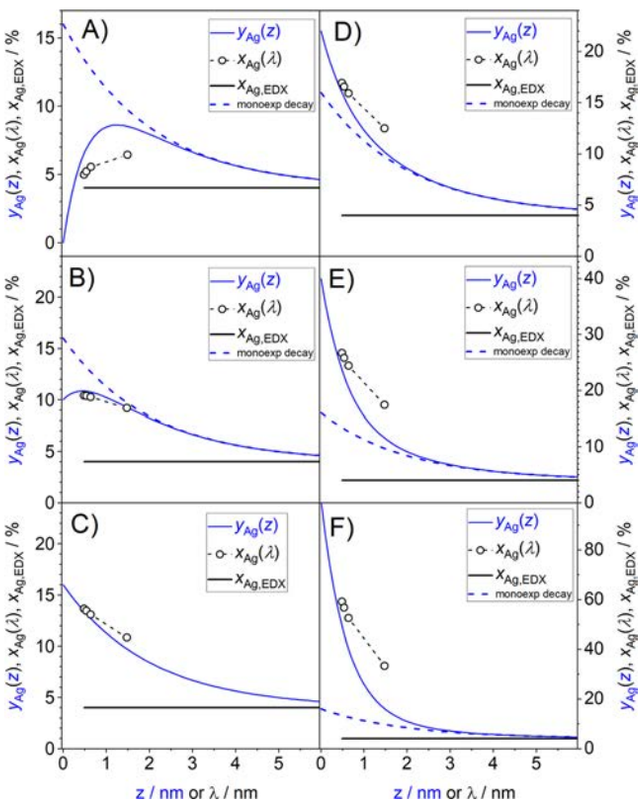

Figure 9. Comparison of assumed biexponential concentration profiles $y_{Ag}(z)$ (solid blue lines) to *calculated* photoelectron intensities $x_{Ag}(\lambda)$ for different ineleastic mean free path length $\lambda(\Upsilon)$ and EDX intensities (horizontal black line). $y_{Ag}(z)$ was calculated according to eq S5 with the parameters given in Table S5. The constant bulk value was $y_{Ag}{}^{*}$ = 4%, the preexponential factor $y^{0}{}_{Ag,1}$ = 12%, and the decay length of the concentration profiles were β_1 = 2.000 nm and β_2 = 0.574 nm. The second preexponential factor $y^{0}{}_{Ag,2}$ was varied: (A) −16% (topmost layer is pure Au), (B) −6%, (C) 0 (i.e., monoexponential decay), (D) +6%, (E) +24%, and (F) +84% (topmost layer is pure Ag). Dashed blues lines are a monoexponential concentration profile for comparison, and dashed black lines are a guide to the eye.

CONCLUSIONS

The amount and distribution of residual Ag in NPG obtained from dealloying Ag−Au alloys bear important implications for electrocatalysis such as methanol oxidation in alkaline solution. The use of alkaline solutions retards further Ag dissolution and coarsening during electrochemical methanol oxidation as compared to similar treatments in acidic solutions. Here we tested the influence of thermal and electrochemical treatments on the amount and distribution of residual Ag in NPG that may impact methanol oxidation and other electrocatalytic applications. Using XPS, we detected a major compositional change during the thermal annealing, linked to a surface segregation of residual Ag. The compositional change starts at around 100 °C when Ag oxides thermally decompose. However, major changes of surface Ag mole fraction require higher temperatures that also cause coarsening of the ligaments involving the rearrangement of a large number of atoms.

A further nondestructive depth profiling of residual Ag in NPG samples by means of synchrotron radiation photo electron spectroscopy experiments after different electro chemical and thermal treatments confirmed the surface segregation in the near surface layers of each ligament. The surface enrichment factor $x_{Ag,XPS}/x_{Ag,EDX}$ increases with decreasing overall Ag content. However, our data neither confirmed nor excluded a further systematic enrichment or depletion of silver in the topmost atomic layer for NPG subjected to thermal treatment or to different potential programs in KOH solution and alkaline methanol solution after the dealloying. Such changes in the topmost atomic layer could be very relevant for electrocatalytic applications. Based on those data, surface concentrations derived from EDX and even XPS intensities by using the model of homogeneous alloys provides reasonable estimations of near surface composition within the uncertainty ranges of the methods themselves. However, the Ag concentration in the topmost layer may still deviate considerably without leaving undis putable signatures even in SXPS data.

ASSOCIATED CONTENT

SI 1: analysis of species desorbed during thermal treatment in vacuum; SI 2: additional SEM images for annealed samples; SI 3: cyclic voltammetry of NPG in alkaline methanol solution; SI 4: SEM images of samples used for SXPS measurements; SI 5: details of the quantitative evaluation of the SXP spectra; SI 6: details of quantitative treatment of XP spectra; SI 7: calculation of SXPS and XPS intensities for assumed concentration profiles (PDF)

AUTHOR INFORMATION

Corresponding Author

Gunther Wittstock − *Carl von Ossietzky University of Oldenburg, Chemistry Department, 26111 Oldenburg, Germany;* orcid.org/0000 0002 6884 5515; Email: wittstock@uol.de

Authors

Mareike Haensch − *Carl von Ossietzky University of Oldenburg, Chemistry Department, 26111 Oldenburg, Germany;* orcid.org/0000 0002 5737 4017

Matthias Graf − *Helmholtz Center Geesthacht, Institute for Materials Research, Materials Technology, 21502 Geesthacht, Germany;* orcid.org/0000 0002 2065 0014

Weijia Wang − *Karlsruhe Institute of Technology, Institute of Functional Interfaces, 76344 Eggenstein Leopoldshafen, Germany;* orcid.org/0000 0003 0602 8162

Alexei Nefedov − *Karlsruhe Institute of Technology, Institute of Functional Interfaces, 76344 Eggenstein Leopoldshafen, Germany;* orcid.org/0000 0003 2771 6386

Christof Wöll − *Karlsruhe Institute of Technology, Institute of Functional Interfaces, 76344 Eggenstein Leopoldshafen, Germany;* orcid.org/0000 0003 1078 3304

Jörg Weissmüller − *Helmholtz Center Geesthacht, Institute for Materials Research, Materials Mechanics, 21502 Geesthacht, Germany; Hamburg University of Technology, Institute of Materials Physics and Technology, 21073 Hamburg, Germany;* orcid.org/0000 0002 8958 4414

ACKNOWLEDGMENTS

G.W., M.H., and J.W. thank Deutsche Forschungsgemeinschaft (DFG) for funding within Research Group FOR2213 255613253 (subprojects 3 (J.W.) and 4 (G.W.)). A.N., W.W., and C.W. gratefully acknowledge support by "Science and Technology of Nanosystems" Programme (Project No. 432202) of Helmholtz Association. W.W. is also grateful for a Postdoctoral fellowship donated by the Helmholtz and China Postdoctoral Council (OCPC). M.G. is funded by DFG within SFB986, Project 192346071. The authors also thank Helmholtz Zentrum Berlin for the allocation of synchrotron radiation beam time at BESSY II.

REFERENCES

(1) Kramer, D.; Viswanath, R. N.; Weissmüller, J. Surface Stress Induced Macroscopic Bending of Nanoporous Gold Cantilevers. *Nano Lett.* **2004**, *4*, 793−796.

(2) Biener, J.; Wittstock, A.; Zepeda Ruiz, L. A.; Biener, M. M.; Zielasek, V.; Kramer, D.; Viswanath, R. N.; Weissmüller, J.; Bäumer, M.; Hamza, A. V. Surface chemistry driven actuation in nanoporous gold. *Nat. Mater.* **2009**, *8*, 47−51.

(3) Lang, X. Y.; Yuan, H. T.; Iwasa, Y.; Chen, M. W. Three dimensional nanoporous gold for electrochemical supercapacitors. *Scr. Mater.* **2011**, *64*, 923−926.

(4) Huang, J. F. Facile preparation of an ultrathin nickel film coated nanoporous gold electrode with the unique catalytic activity to oxidation of glucose. *Chem. Commun. (Cambridge, U. K.)* **2009**, 1270−1272.

(5) Ge, X.; Wang, L.; Liu, Z.; Ding, Y. Nanoporous Gold Leaf for Amperometric Determination of Nitrite. *Electroanalysis* **2011**, *23*, 381−386.

(6) Graf, M.; Haensch, M.; Carstens, J.; Wittstock, G.; Weissmüller, J. Electrocatalytic methanol oxidation with nanoporous gold: Microstructure and Selectivity. *Nanoscale* **2017**, *9*, 17839.

(7) Wittstock, A.; Biener, J.; Bäumer, M. Surface chemistry and catalysis. *RSC Nanosci. Nanotechnol.* **2012**, *22*, 167−198.

(8) Hu, K.; Ziehmer, M.; Wang, K.; Lilleodden, E. T. Nanoporous gold: 3D structural analyses of representative volumes and their implications on scaling relations of mechanical behaviour. *Philos. Mag.* **2016**, *96*, 3322−3335.

(9) Graf, M.; Roschning, B.; Weissmüller, J. Nanoporous Gold by Alloy Corrosion: Method Structure Property Relationships. *J. Electro chem. Soc.* **2017**, *164*, C194−C200.

(10) Mahr, C.; Kundu, P.; Lackmann, A.; Zanaga, D.; Thiel, K.; Schowalter, M.; Schwan, M.; Bals, S.; Wittstock, A.; Rosenauer, A. Quantitative determination of residual silver distribution in nano porous gold and its influence on structure and catalytic performance. *J. Catal.* **2017**, *352*, 52−58.

(11) Seo, B.; Kim, J. Electrooxidation of Glucose at Nanoporous Gold Surfaces: structure Dependent Electrocatalysis and Its Application to Amperometric Detection. *Electroanalysis* **2010**, *22*, 939−945.

(12) Fujita, T.; Guan, P.; McKenna, K.; Lang, X.; Hirata, A.; Zhang, L.; Tokunaga, T.; Arai, S.; Yamamoto, Y.; Tanaka, N.; Ishikawa, Y.; Asao, N.; Yamamoto, Y.; Erlebacher, J.; Chen, M. Atomic origins of the high catalytic activity of nanoporous gold. *Nat. Mater.* **2012**, *11*, 775−780.

(13) Wittstock, A.; Biener, J.; Bäumer, M. Introduction to nanoporous gold. *RSC Nanosci. Nanotechnol.* **2012**, *22*, 1−10.

(14) Krekeler, T.; Straßer, A. V.; Graf, M.; Wang, K.; Hartig, C.; Ritter, M.; Weissmüller, J. Silver rich clusters in nanoporous gold. *Mater. Res. Lett.* **2017**, *5*, 314−321.

(15) Moskaleva, L. V.; Röhe, S.; Wittstock, A.; Zielasek, V.; Klüner, T.; Neyman, K. M.; Bäumer, M. Silver residues as a possible key to a remarkable oxidative catalytic activity of nanoporous gold. *Phys. Chem. Chem. Phys.* **2011**, *13*, 4529−4539.

(16) Hoppe, S.; Li, Y.; Moskaleva, L. V.; Mueller, S. How silver segregation stabilizes 1D surface gold oxide: A cluster expansion study combined with ab initio MD simulations. *Phys. Chem. Chem. Phys.* **2017**, *19*, 14845−14853.

(17) Yin, H.; Zhou, C.; Xu, C.; Liu, P.; Xu, X.; Ding, Y. Aerobic oxidation of D glucose on support free nanoporous gold. *J. Phys. Chem. C* **2008**, *112*, 9673−9678.

(18) Zielasek, V.; Juergens, B.; Schulz, C.; Biener, J.; Biener, M. M.; Hamza, A. V.; Bäumer, M. Gold catalysts: Nanoporous gold foams: Nanoporous gold foams. *Angew. Chem., Int. Ed.* **2006**, *45*, 8241−8244.

(19) Wittstock, A.; Neumann, B.; Schaefer, A.; Dumbuya, K.; Kuebel, C.; Biener, M. M.; Zielasek, V.; Steinrueck, H. P.; Gottfried, J. M.; Biener, J.; Hamza, A.; Bäumer, M. Nanoporous Au: An Unsupported Pure Gold Catalyst? *J. Phys. Chem. C* **2009**, *113*, 5593−5600.

(20) Personick, M. L.; Zugic, B.; Biener, M. M.; Biener, J.; Madix, R. J.; Friend, C. M. Ozone Activated Nanoporous Gold: A Stable and Storable Material for Catalytic Oxidation. *ACS Catal.* **2015**, *5*, 4237−4241.

(21) Zugic, B.; Wang, L.; Heine, C.; Zakharov, D. N.; Lechner, B. A. J.; Stach, E. A.; Biener, J.; Salmeron, M.; Madix, R. J.; Friend, C. M. Dynamic restructuring drives catalytic activity on nanoporous gold silver alloy catalysts. *Nat. Mater.* **2017**, *16*, 558−564.

(22) Schaefer, A.; Ragazzon, D.; Wittstock, A.; Walle, L. E.; Borg, A.; Bäumer, M.; Sandell, A. Toward Controlled Modification of Nanoporous Gold. A Detailed Surface Science Study on Cleaning and Oxidation. *J. Phys. Chem. C* **2012**, *116*, 4564−4571.

(23) Nelson, G. C. Determination of the surface versus bulk composition of silver gold alloys by low energy ion scattering spectroscopy. *Surf. Sci.* **1976**, *59*, 310−314.

(24) Manzhos, R. A.; Krivenko, A. G.; Doronin, S. V.; Choba, M. A.; Safonov, V. A. Surface segregation of silver atoms on Au Ag alloys according to data of laser heating induced temperature potential shifts, XPS and conventional electrochemical methods. *J. Electroanal. Chem.* **2013**, *704*, 175−182.

(25) Tyson, W. R.; Miller, W. A. Surface free energies of solid metals: Estimation from liquid surface tension measurements. *Surf. Sci.* **1977**, *62*, 267−276.

(26) Hoppe, S.; Müller, S. A first principles study on the electronic origins of silver segregation at the Ag Au (111) surface. *J. Appl. Phys.* **2017**, *122*, 235303−9.

(27) Graf, M.; Ngô, B. N. D.; Weissmüller, J.; Markmann, J. X ray studies of nanoporous gold: Powder diffraction by large crystals with small holes. *Phys. Rev. Mater.* **2017**, *1*, 98.

(28) Band, I. M.; Kharitonov, Y. I.; Trzhaskovskaya, M. B. Photoionization Cross Sections and Photoelectron Angular Distribu tion for X ray Line Energies in the Range 0.132 4.509 keV. *At. Data Nucl. Data Tables* **1979**, *23*, 443.

(29) Shinotsuka, H.; Tanuma, S.; Powell, C. J.; Penn, D. R. Calculations of electron inelastic mean free paths. X. Data for 41 elemental solids over the 50eV to 200 keV range with the relativistic full Penn algorithm. *Surf. Interface Anal.* **2015**, *47*, 871−888.

(30) Nečas, D.; Klapetek, P. Gwyddion: an open source software for SPM data analysis. *Cent. Eur. J. Phys.* **2012**, *10*, 181−188.

(31) Hodge, A. M.; Hayes, J. R.; Caro, J. A.; Biener, J.; Hamza, A. V. Characterization and Mechanical Behavior of Nanoporous Gold. *Adv. Eng. Mater.* **2006**, *8*, 853−857.

(32) Schon, G.; Tummavuori, J.; Lindstrom, B.; Enzell, C. R.; Enzell, C. R.; Swahn, C. G. ESCA studies of Ag, Ag_2O and AgO. *Acta Chem. Scand.* **1973**, *27*, 2623−2633.

(33) Tyson, C. C.; Bzowski, A.; Kristof, P.; Kuhn, M.; Sammynaiken, R.; Sham, T. K. Charge redistribution in gold silver alloys from a local perspective. *Phys. Rev. B* **1992**, *45*, 8924−8928.

(34) Waterhouse, G. I. N.; Bowmaker, G. A.; Metson, J. B. The thermal decomposition of silver (I, III) oxide: A combined XRD, FT IR and Raman spectroscopic study. *Phys. Chem. Chem. Phys.* **2001**, *3*, 3838−3845.

(35) Li, R.; Sieradzki, K. Ductile Brittle Transition in Random Porous Au. *Phys. Rev. Lett.* **1992**, *68*, 1168−1171.
(36) Defay, R.; Prigogine, I. *Surface Tension and Adsorption*; Wiley: New York, 1966.
(37) Lackmann, A.; Bäumer, M.; Wittstock, G.; Wittstock, A. Independent control over residual silver content of nanoporous gold by galvanodynamically controlled dealloying. *Nanoscale* **2018**, *10*, 17166−17173.
(38) Zhang, J.; Liu, P.; Ma, H.; Ding, Y. Nanostructured Porous Gold for Methanol Electro Oxidation. *J. Phys. Chem. C* **2007**, *111*, 10382−10388.